

Sensor and Simulation Notes

Note 329

PL/PA 5/19/95

Analysis of the Impulse Radiating Antenna

Everett G. Farr

July 24, 1991

Abstract

One form of Impulse Radiating Antenna (IRA) combines the technologies of the Balanced Transmission-line Wave (BTW) sensor with TEM-fed paraboloidal reflector antennas. The behavior of the IRA was calculated using a combination of the Method of Moments, using the NEC Code, and Geometrical Optics. The results of NEC compare favorably to both high and low frequency asymptotes. The frequency domain results were driven by an inverse double exponential step function, in order to find the time domain radiated far field.

PI 96-1253

## I. Introduction

There has recently been interest in radiating broadband pulses of electromagnetic energy. Such a phenomenon is useful in a variety of applications, one of which is in a radar system that looks at the ground from the air. One of the more difficult problems with such a system, however, has been in finding a suitable antenna. This is due not only to the very wide bandwidth of interest, but also to the necessity of preserving the shape of the pulse into the far field. One candidate for such an antenna is the Impulse Radiating Antenna (IRA). The purpose of this report is to analyze the properties of the IRA, and to provide a basis for comparison to other candidate antennas.

The problem of how to radiate an impulse is difficult for a number of reasons. Antenna designs normally need to span only a relatively narrow bandwidth, however, the antenna we needed had to span two full decades of frequency; from about 20 MHz to 2 GHz. The classical method of radiating broadband signals involves structures such as the log periodic antennas commonly used in television antennas. Although these are broadband antennas, they have the drawback of being dispersive. Thus, the high frequencies arrive at a target at a different time than the low frequencies, so the shape of the impulse is not preserved. Another possible candidate for radiating an impulse is the TEM horn.<sup>1</sup> Although this antenna is nondispersive, it has the drawback that the phase front at the end of the antenna is spherical, not planar, unless a lens is used. Maximum gain is achieved by having a planar phase front. In order to make the phase front on a TEM horn as planar as possible, it is necessary to build the horns with lengths that are large compared to the dimensions of their apertures. Thus, a long antenna is required to maintain a planar phase front.

Another way to handle the problem is to force the phase front to be planar by focusing it with a parabolic dish. This is the approach the IRA uses. The IRA was first proposed by C. Baum<sup>2,3,4</sup> as a technique for radiating high frequencies with a TEM-fed dish, while doing the best one can with the low frequencies by using a Balanced Transmission-line Wave (BTW) sensor<sup>5,6,7</sup> as an integrated feed. Thus, the IRA can be considered a blending of the two technologies of dish antennas and BTWs. The BTW has an output on boresight similar to a magnetic loop of the same area. It is different off boresight, however, in that a magnetic loop has a pattern of  $\cos \theta$ , while the BTW has pattern of  $1 + \cos \theta$ . Thus, the BTW provides some directionality even at frequencies where the antenna is small compared to wavelength.

A diagram of an IRA is shown in Figure 1. This diagram shows an IRA for a single polarization, however, we could achieve dual polarization by adding a second pair of feed arms perpendicular to the first set. This would allow two arms to be charged positive and two negative. One could alter the excitation to achieve both horizontal and vertical polarizations. A diagram of this dual polarization arrangement is shown in Figure 2. Note that it is preferable to drive the antenna with 2 pairs of arms rather than just one. This is because the input impedance with two pairs of arms driven is half the input impedance with a single pair of arms driven. This decrease in input impedance leads to a radiated far field increase of  $\sqrt{2}$ , assuming a constant voltage at the source.



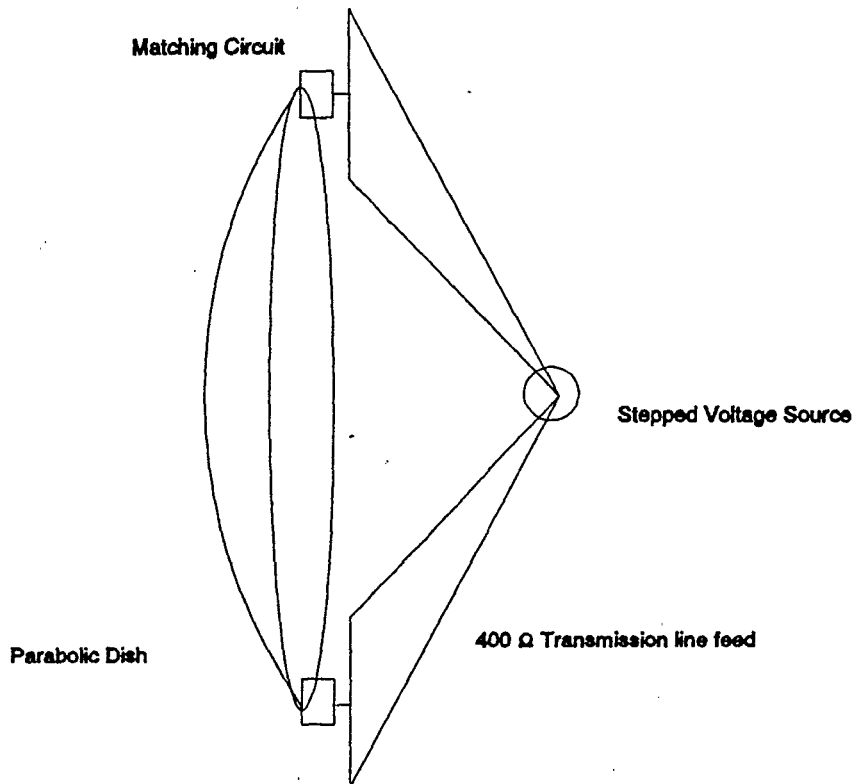


Figure 1. The Impulse Radiating Antenna (IRA)

Note also that the fields generated by a single pair of arms are orthogonal to those generated by the other pair. This allows us to analyze the IRA as a device with a single pair of arms. If we want to add the second pair of arms to the analysis, we simply rotate the dish by 90 degrees, and add the fields using the principle of superposition.

To describe the performance of the IRA, a number of analysis methods were considered, including both time and frequency domain techniques. Among the time domain techniques were a Finite Difference Time Domain code and the Thin Wire Time Domain code. Among the frequency domain methods were the Method of Moments and Geometrical Optics. All the techniques have their advantages and disadvantages, but some are easier to implement than others. In particular, it was felt that both of the time domain techniques would require either a very small cell size or a very short wire length in order to adequately describe the geometry, due to the 250 ps risetime of the driving voltage. There is an additional difficulty in describing a smooth reflector with blocks, since blocks will not be conformal with the surface of the dish.

Thus, we felt that a frequency domain method that used different approaches at low and high frequencies would be more suitable. At low frequencies we used the Method of Moments (MoM) as implemented in the Numerical Electromagnetics Code (NEC). This code

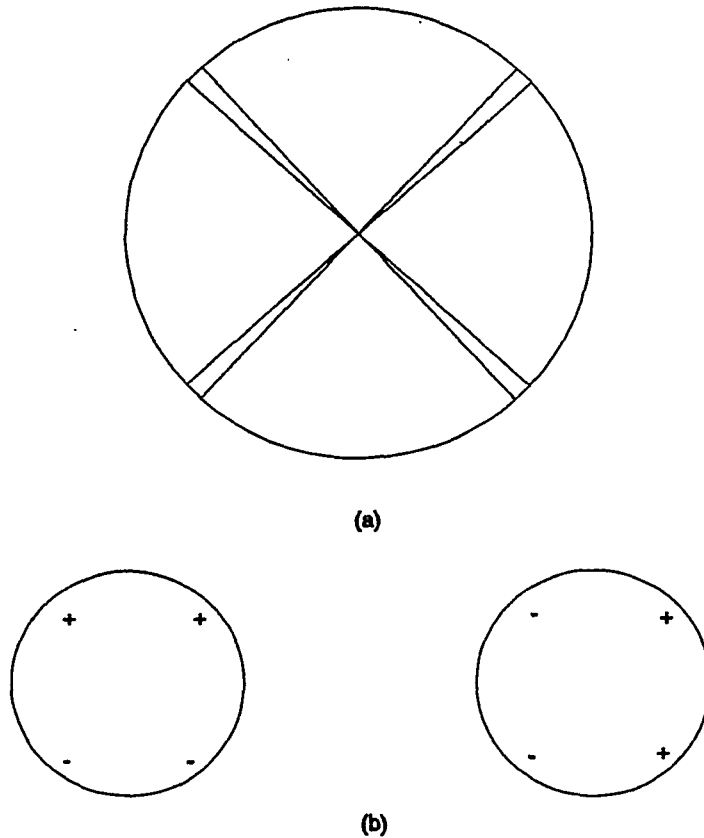


Figure 2. Feed arms for a dual polarized IRA (a) and two orthogonal methods of feeding it (b)

models the structure with thin wires, circuit elements, and voltage sources. At high frequencies we used Geometrical Optics (GO), since the behavior of the IRA is similar to a standard dish at these frequencies. Once we had the frequency response over the low and high ends of the frequency range, we drove the antenna with a time domain voltage and used a Fast Fourier Transform (FFT) to get a time domain response.

In addition to MoM and GO, we were able to draw an analogy between the IRA and a magnetic loop at low frequencies. Thus, the three techniques we considered involved a low-frequency asymptote with a magnetic loop analysis, a high frequency asymptote with Geometrical Optics, and the Numerical Electromagnetics Code to tie the two together. We begin now with the low frequency analysis.

## II. Low Frequency Analysis

In order to understand the low-frequency behavior of the IRA, it is first necessary to understand the BTW. Although a detailed outline is provided in Reference 5, we review the BTW's properties briefly here.

Diagrams of the BTW are shown in Figure 3 and 4. It is very similar to a transmission line with matched loads at either end. Consider a plane wave incident from the right upon the structure of Figure 3b. The electric field drives either end of the structure similarly, i.e., with the same polarization. The mechanism here is like inducing a voltage on a parallel-plate capacitor in a changing electric field. The magnetic field, however, drives the two ends of transmission line oppositely. The mechanism here is like that of driving current around a loop with a changing magnetic field.

It is shown in [5] that the charges induced on the end nearest the incident field add, while they cancel on the opposite end. This cancellation occurs as long as the wave on the transmission line propagates at the speed of light. In practice, this means that there is little or no dielectric material near the two plates.

When the BTW is in transmit mode, one needs to drive the end closest to the desired direction of radiation. The radiated field on axis is the same as a loop with an area equal to the cross section of the transmission line as viewed from the side. Again, this is demonstrated in [5].

If we consider once again the IRA of Figure 1, we see that the feed section is just a transmission line, although now it is in spherical rather than rectangular coordinates. Remembering that the BTW radiates in the direction closest to the feed, we see that the low frequencies are radiated in the correct direction; the same direction as the high frequencies are radiated after reflection off the dish.

It is shown in [5] that it is necessary for the transmission line to be matched correctly in order to have behavior like a BTW. This can be approximated by using a resistance equal to the characteristic impedance of the feed structure, or 200  $\Omega$  on each arm. This is only an approximation, however, because of the additional capacitance due to the reflector. In practice, it will be necessary to match the load using either a TDR or an antenna measurement to minimize the backlobe.

Let us return now to the IRA of Figure 1. The radiated field for a loop is found to be

$$E(\omega) = \frac{e^{-jkr}}{r} K_1 (j\omega)^2 V(\omega) \quad (1)$$

in the frequency domain, or

$$E(t) = \frac{K_1}{r} \frac{d^2}{dt^2} V(t) \quad (2)$$

in the time domain, where

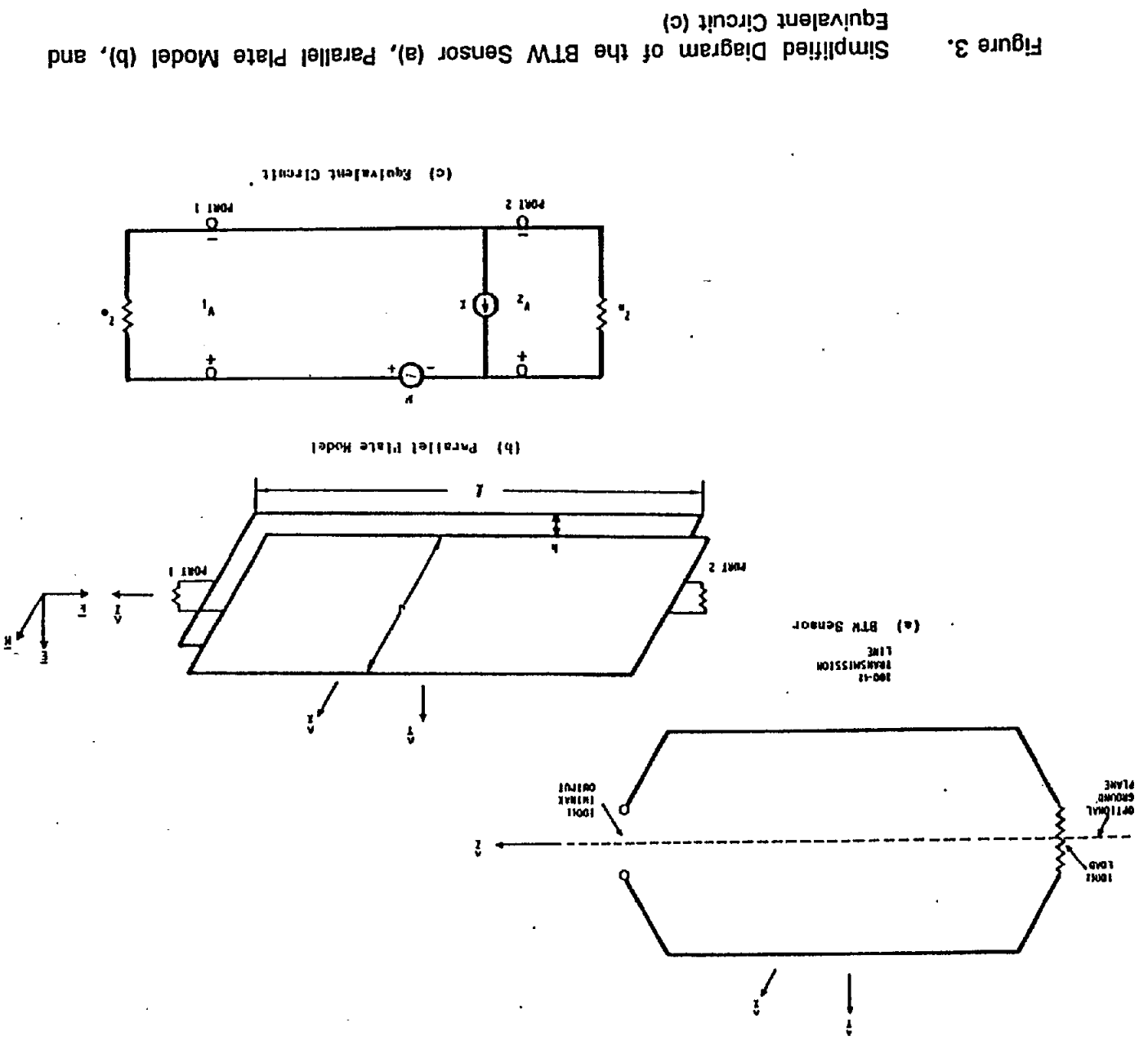


Figure 3. Simplified Diagram of the BTW Sensor (a), Parallel Plate Model (b), and Equivalent Circuit (c)

7

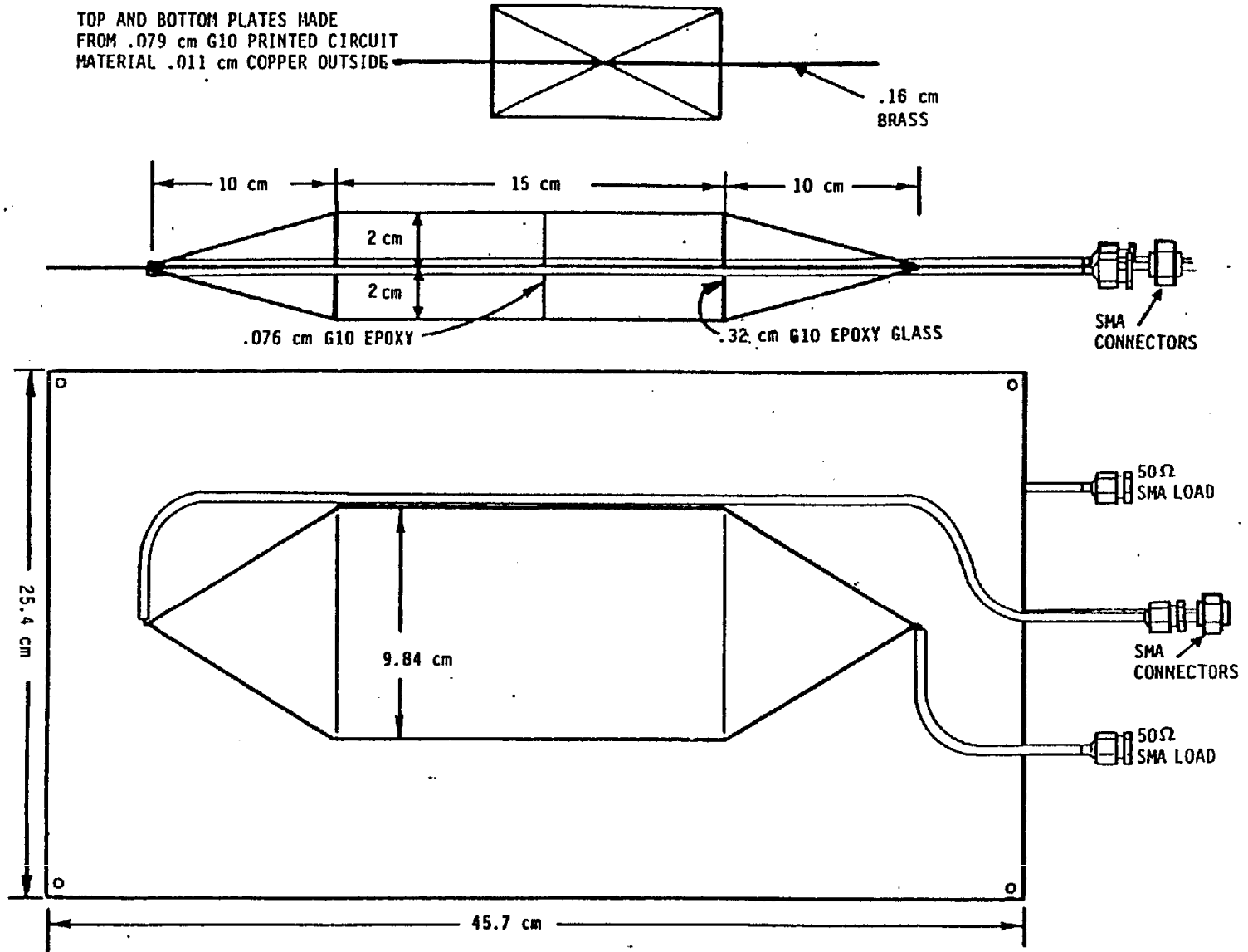


Figure 4. Diagram of the BTW

$$K_1 = \frac{\eta A}{Z_c 4 \pi c^2} \quad (3)$$

In the above equation,  $\eta$  is the characteristic impedance of free space,  $Z_c$  is the characteristic impedance of the feed section (400  $\Omega$ ), and  $c$  is the speed of light. Thus, the output at low frequencies is just the second derivative of the input voltage, times a constant.

Let us now assign some typical numbers to the above equations. If we assume  $F/D = 0.4$ , and the dish radius,  $b = 0.6$  m, then we find the area through the loop,  $A$ , to be 0.251 m<sup>2</sup> and  $K_1 = 2.01 \times 10^{-19}$  sec<sup>2</sup>. Hence, we have a simple expression of the expected behavior at the low frequencies. The output is proportional to frequency squared. Off-axis, this analysis has to be modified by a  $1 + \cos \theta$  factor. The above analysis is valid approximately up to a frequency where the length of the transmission line is less than or equal to  $\lambda/2\pi$ . This constraint was first provided by C. Baum<sup>8</sup>. Thus, for our configuration, the magnetic loop analogy is valid up to about 80 MHz. At higher frequencies it is necessary to use either the Method of Moments (with NEC) or Geometrical Optics.

We should note here that the above analysis has some ambiguity built into it. The area of the loop is not really a well-defined quantity, since current flowing from one arm to the other can flow through either the center of the dish or around its rim. It seems that some current will flow everywhere on the dish, so we have used the average of these two areas.

### III. High Frequency Analysis: Geometrical Optics

The next step in the analysis is to generate the high frequency asymptote of the radiated field. One of the benefits of breaking the problem into high and low frequency regions, is that the high frequency technique we use, Geometrical Optics (GO), is very simple to implement in the frequency domain. Indeed, in the frequency domain, the problem becomes easier at higher frequencies, since GO is most valid when surfaces are large compared to the wavelength. By contrast, time domain solutions become more difficult at higher frequencies (faster risetimes), due to a requirement for a minimum number of cells or wire segments per wavelength.

If we have a source at the focus of a parabolic dish, it will project a plane wave in front of the dish. Thus, we need to find the field radiated from an aperture in a plane in front of the dish. The geometry is shown in Figure 5. In the plane  $z=0^s$ ,

$$E_\theta = j\omega \frac{e^{-jkr}}{2\pi rc} (P_x \cos\phi + P_y \sin\phi) \quad (4)$$

$$E_\phi = j\omega \frac{e^{-jkr}}{2\pi rc} \cos\theta (P_y \cos\phi - P_x \sin\phi) \quad (5)$$

where

$$P_x = \iint_S E_{ax}(x,y) e^{-\frac{j\omega}{c}(x'\sin\theta\cos\phi + y'\sin\theta\sin\phi)} dx' dy' \quad (6)$$

$$P_y = \iint_S E_{ay}(x,y) e^{-\frac{j\omega}{c}(x'\sin\theta\cos\phi + y'\sin\theta\sin\phi)} dx' dy' \quad (7)$$

On boresight, where  $\theta = 0$ , the above simplifies to

$$E_\theta = j\omega \frac{e^{-jkr}}{2\pi rc} \iint_S E_y(x',y') dx dy \quad (8)$$

In the above equations, it is necessary to generate an aperture field,  $E_a(x',y',\omega)$ . This is approximated by the cross sectional field of a transmission line consisting of two parallel cables set apart by the diameter of the dish and with a radius appropriate to keeping the impedance at  $400 \Omega$ . Since all the rays originating from a focus arrive at the aperture plane at the same time, the aperture function is of the form

$$E_{ap}(x,y) = E_o f(t) g(x,y) \quad (9)$$

where  $E_o$  is the field at the center of the aperture,  $g(x,y)$  is the variation within the aperture, and  $f(t)$  is the time variation of the aperture electric field, and consequently, the variation of the voltage at the apex.

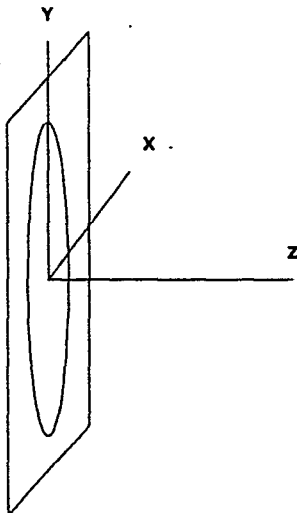


Figure 5. Geometry for Calculating the Radiated Fields Over an Aperture

Another way of thinking about the aperture field calculation is to reflect the feed structure through the dish. Upon doing so, we find it is just two parallel wires arranged so they form a transmission line of  $400 \Omega$  characteristic impedance. A diagram of this is shown in Figure 6. Since the fields for two parallel cylinders are well known, we can approximate the aperture field as being that portion of the field formed by two cylinders that is within the circle formed by the dish.

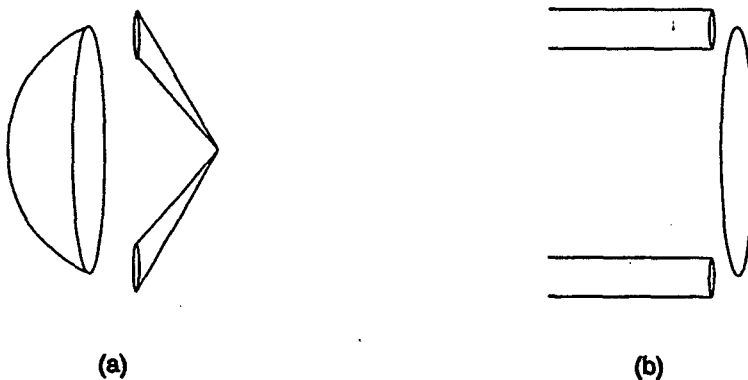


Figure 6. The Effect of Reflecting the Feed Through the Dish. (a) Before Reflection (b) After Reflection

Thus, the aperture field can be found from the field in a two-cylinder transmission line. The characteristic impedance of such a configuration is

$$Z_c = \frac{\eta}{\pi} \cosh^{-1} \frac{b}{f} \quad (10)$$

where  $f$  is the radius of the wires and  $b$  is the height of the wire above a center line. Thus, for a 400  $\Omega$  line, we need  $b/f = 14.03$ . If the radius of our dish is 0.6 m, then  $a = 0.0428$  m.

The field distribution for such an arrangement has been described by C. Baum<sup>10</sup>. A diagram of the fields is shown in Figure 7, which is taken from [6]. We find

$$g(x, y) = \frac{1}{2} \left[ \frac{1 + y}{x^2 + (1 + y)^2} + \frac{1 - y}{x^2 + (1 - y)^2} \right] \quad (11)$$

which has been normalized to  $\sqrt{b^2 - f^2} = 1$ , where  $b$  is the dish radius and  $f$  is the wire radius. Furthermore, the field at the center of the dish is

$$E_o = \frac{V_o}{\sqrt{b^2 - f^2} \cosh^{-1} \frac{b}{f}} \quad (12)$$

By using these aperture fields, we can perform the integrals of Equation 8 numerically. Thus, we find

$$E(\omega) = j\omega \frac{e^{-jkr}}{r} K_2 V(\omega) \quad (13)$$

in the frequency domain, or

$$E(t) = \frac{K_2}{r} \frac{d}{dt} V(t) \quad (14)$$

in the time domain, where

$$K_2 = \frac{0.90}{2\pi} \frac{b}{c} \quad (15)$$

and  $c$  is the speed of light.

This expression for  $K_2$  is specific for a 400 Ohm feed. Thus we find for  $b = 0.6$  m,  $K_2 = 2.86 \times 10^{-10}$  sec. This rather simple result indicates that the output of the IRA at high frequencies is proportional to frequency, or to the derivative of the input voltage.

There are some approximations in our GO solution. When we integrated the field over the aperture, we used conical feed arms to generate the aperture field instead of the flat plates that will likely be used in the final design. Although this is an approximation, it should not affect the results very much. Another approximation we used is that we ignored diffraction from the edge of the dish. Edge diffraction is not normally significant in the main beam, however, so it will not have a strong effect on our analysis. Finally, we ignored

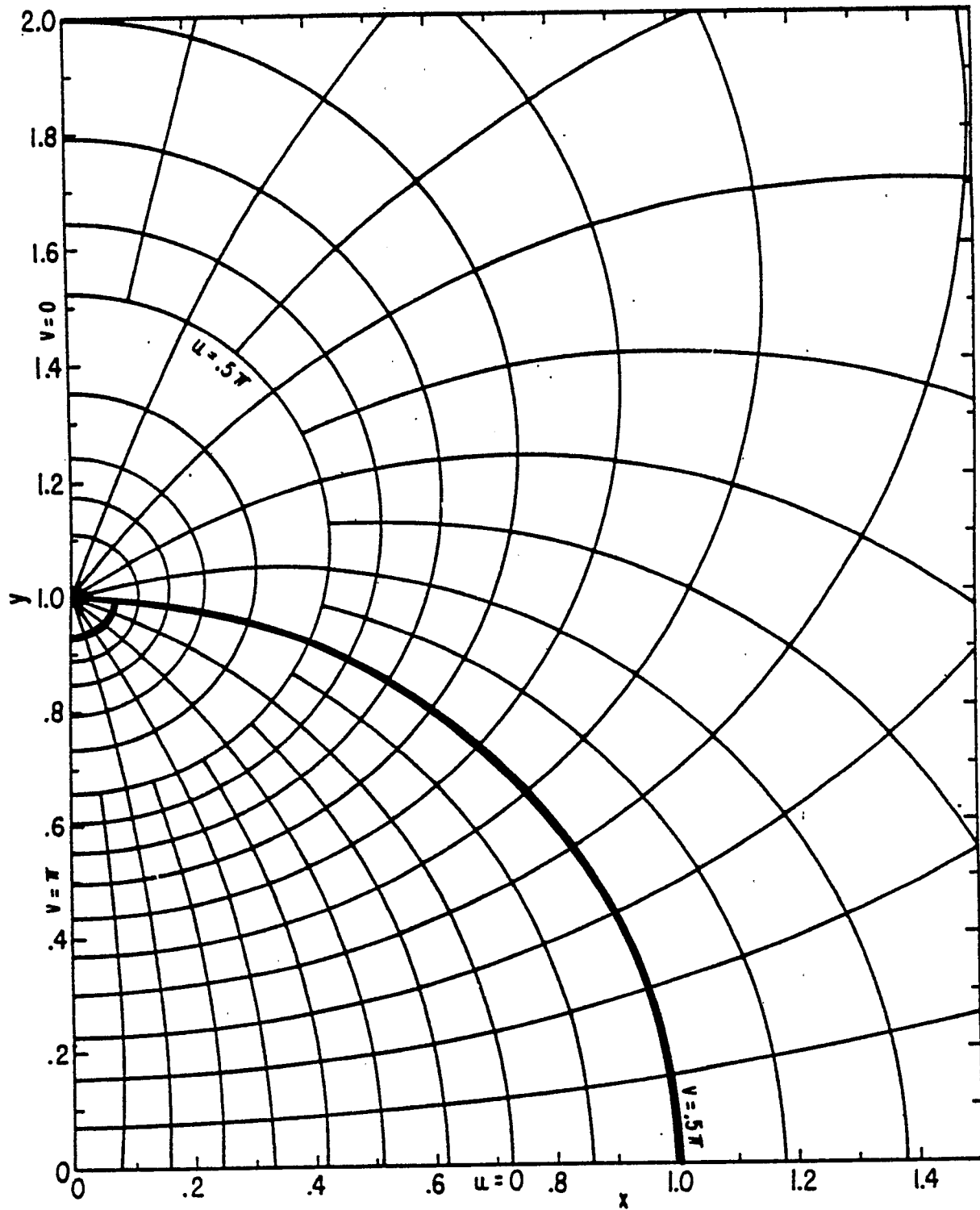


Figure 7. Lines of constant E- and H-Fields for a Two-Wire Transmission Line (from<sup>[6]</sup>)

aperture blockage due to the feed structure. This can be minimized, however, by shaping the feed arms properly.

Let us consider how best to shape the feed arms to minimize aperture blockage. Three variations on the shape of the feed arms are shown in Figure 8. One can have either conical arms, or one can have triangle-shaped plates in either the plane of symmetry or perpendicular to it. By laying the plate in the plane of symmetry, as shown in Figure 8c, the aperture field is disturbed as little as possible. It has been demonstrated by D. Giri and C. Baum that when a plate is sufficiently high above a ground plane, the fields can be approximated by a cylinder whose diameter is half the strip width<sup>11</sup>. One can use this fact to determine the appropriate angles for the edges of the plates.

It is of some interest at this point to calculate the amount of energy that is lost due to aperture spillage. We can calculate this by integrating the field over the aperture, and comparing the power in the integrated field to the power in the driving voltage. Thus we find the aperture efficiency to be

$$e = \frac{1/\eta \int \int_{\lambda} E_y^2(x, y) dS}{V^2/Z_c} \quad (16)$$

The integral was carried out numerically, using the expressions for the electric field provided above. We found for our test configuration an aperture loss of 4.5 dB. This calculation is independent of the F/D ratio and the aperture diameter. It is dependent upon the characteristic impedance of the feed structure, however, it is likely that this will remain as 400  $\Omega$ .

In conclusion, we see that the high-frequency portion of the analysis leads to a simple result; that the radiated waveform is proportional to the derivative of the input voltage. The next step in the analysis is to tie the high and low frequency asymptotes together with a numerical code.

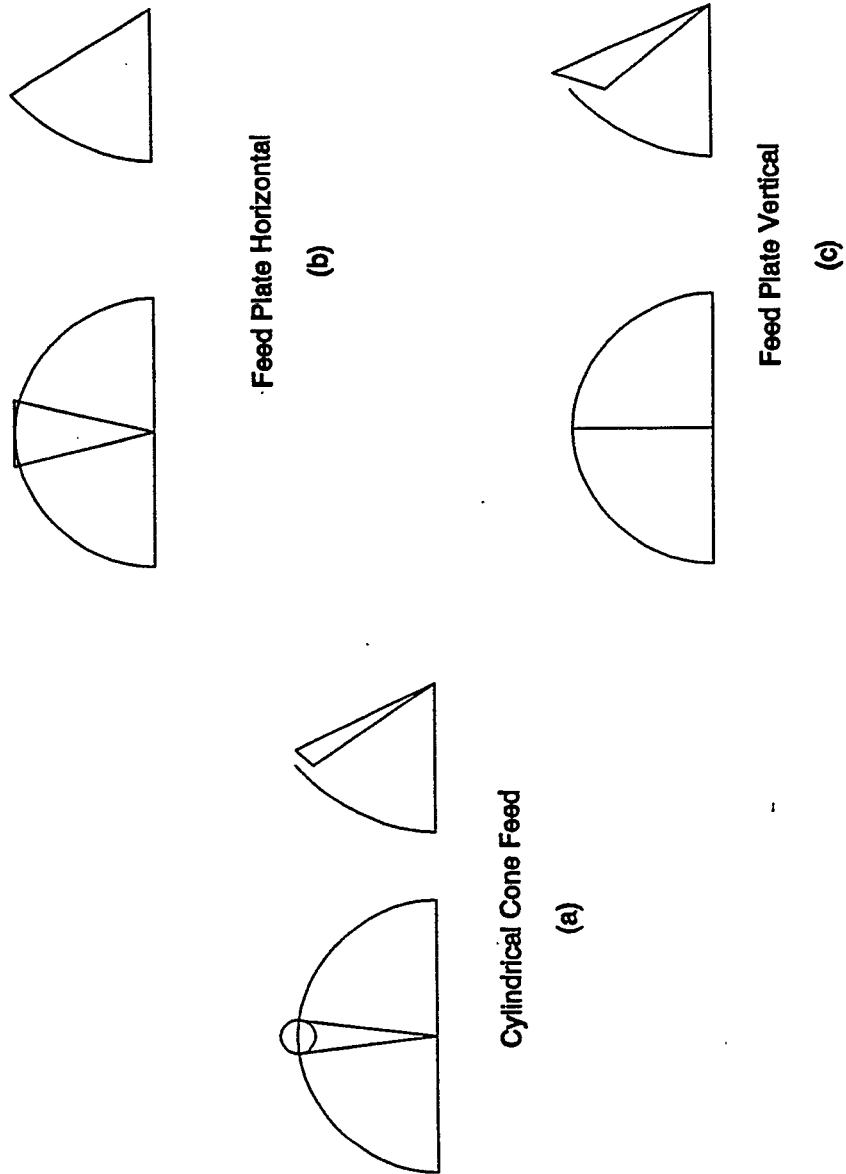


Figure 8. Various Choices for the Shape of the Feed Arms

#### IV. Intermediate-Frequency Analysis: Method of Moments

We can tie the high- and low-frequency results together by using the Method of Moments as implemented by the computer code NEC<sup>12</sup>. Although it becomes difficult to use NEC much higher than 200 MHz, it is helpful to see what happens below there. NEC, as it is being used here, is a code that models a structure as a collection of thin wires, and can add voltage sources and loads as well. The most important limitation on the use of NEC is that it can only work for wires that are short compared to a wavelength at the frequency of interest. Thus, there is an upper limit on the frequencies we can study with NEC.

A diagram of the wire structure used to simulate the IRA is shown in Figure 9. Although the mesh is somewhat sparse, we are able to achieve reasonable results up into the region where the high frequency solution holds. NEC was run for both a tapered feed and for a uniform feed. Although the tapered feed is a better representation of the actual feed, there may be numerical problems with continuity of the current at the junction of wires of different radii.

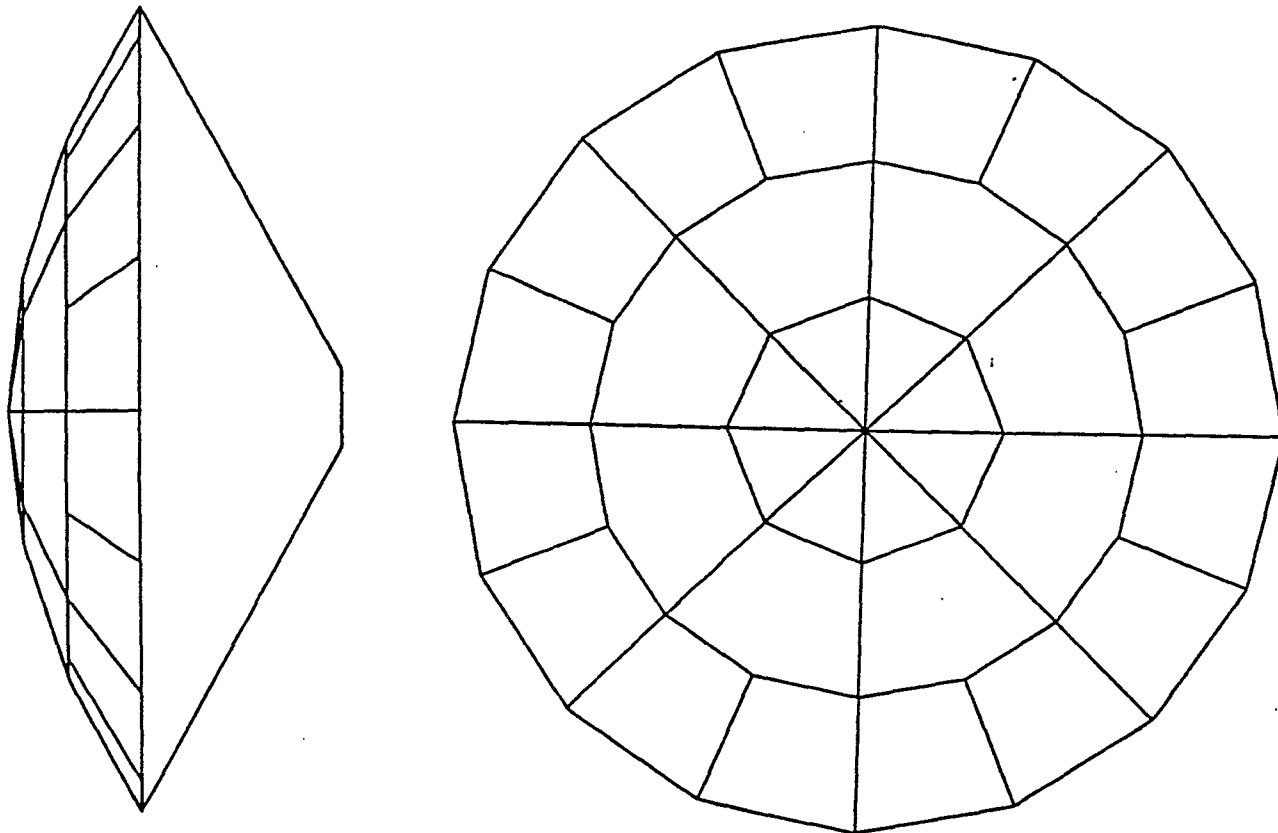


Figure 9. Wire Structure Used for the NEC Modeling

The diameter of the dish was 0.6 m and the F/d ratio was 0.4. A voltage source was at the focus of the reflector. The radii of all the wires in the reflector were 12 mm, as were the wire radii in the feed with straight sections. With the tapered feed, the wire diameters went from 4.26 mm to 38.34 mm in five sections. The section of the feed closest to the reflector was loaded with a 200  $\Omega$  resistance. The extended thin-wire kernel was used in NEC in order to enhance accuracy.

A graph of the output of NEC appears in Figure 10, along with the calculations of the high- and low-frequency approximations discussed earlier. It is clear that the NEC results begin to follow the high-frequency approximation at the high end, so we feel confident in the application of Geometrical Optics at higher frequencies. This is necessary in order to provide the conversion to the time domain. At low frequencies, the NEC results are a little higher than the low-frequency asymptote we predicted earlier.

The discrepancy at low frequencies could be explained by several things. One possibility is that our matching circuit is too crude. We used a simple 200  $\Omega$  load there, while we know that there will have to be some reactive elements there to offset the additional capacitance of the dish. A second cause is the ambiguity in the definition of the area of the loop, as discussed in Section II of this report. A third cause might be that too few antenna wires were used when modeling the feed. The feed section was modeled with just four wire segments laid end to end, with successively larger radii. A better approach might be to use a set of wires to model the flat plate that will be the actual shape of the feed.

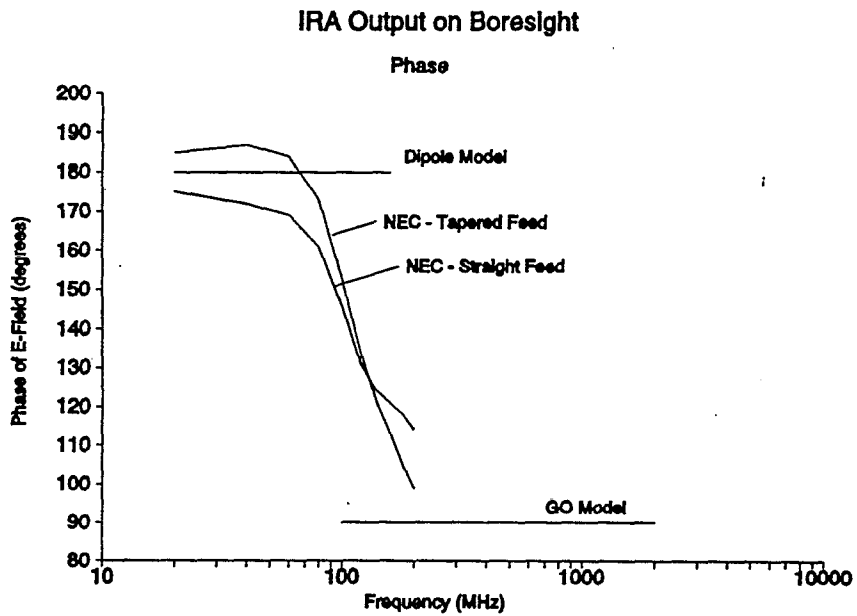
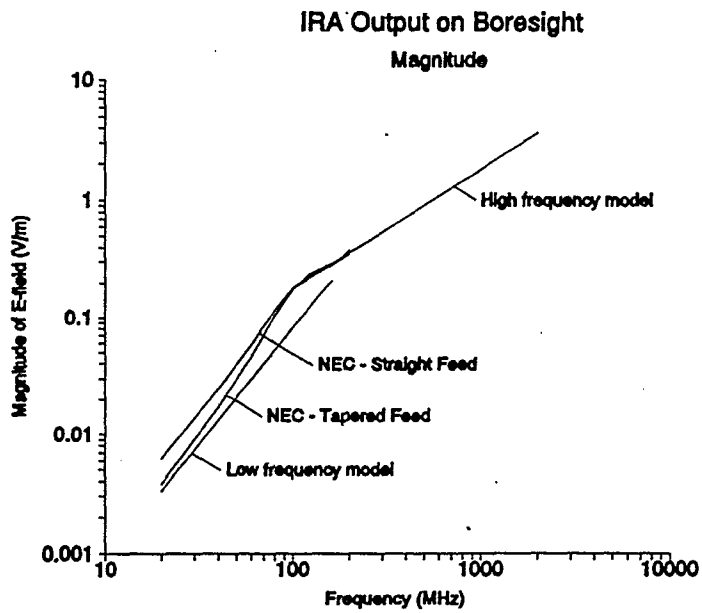


Figure 10. Output of NEC Compared to the High- and Low-Frequency Asymptotes

## V. Time Domain Analysis

Finally, we performed an inverse Fast Fourier Transform (FFT) on the frequency domain result to generate a time domain waveform. We wanted to drive the antenna with a step function, or something that looked similar to it. For numerical reasons, we needed a function with at least a continuous first derivative and an analytic Fourier Transform. Thus we drove the antenna with an inverse double exponential waveform<sup>13</sup> with a fast risetime and slow decay time. It was of the form

$$f(t) = \frac{1}{e^{-(t-t_0)/\tau_r} + e^{(t-t_0)/\tau_d}} \quad (17)$$

where  $t_0 = 20$  ns,  $\tau_r = 56.82$  ps, and  $\tau_d = 217.4$  ns. This gives a 10-90 risetime of 250 ps and a time to decay to 10 % of the peak of 500 ns. A graph of this function is shown in Figure 11.

In order to take the inverse FFT it was necessary to interpolate the frequencies calculated with NEC. We used NEC to calculate frequencies from 20 MHz to 200 MHz in steps of 20 MHz. Above 200 MHz, we extrapolated magnitude proportional to frequency as described in Equation 13, and the phase was forced to 90 degrees. Below 20 MHz we extrapolated magnitude proportional to frequency squared, as described in Equation 180, and the phase was 180 degrees.

A diagram of the resulting time domain waveform is shown in Figure 12. This waveform is normalized to a distance of 1 m and a peak driving voltage of 1 V. We can also plot the magnitude on a logarithmic scale, and this is shown in Figure 13. What we see in the time domain is a small undershoot at early times corresponding to the leading edge, followed by the main portion of the impulse. At later times there is some further undershoot, which may be expected because the integral of the radiated waveform must be zero.

We can get an idea of the accuracy of this technique by looking at the early time waveform. For the time it takes the wavefront to make the round trip between the focus and the reflector, the radiated electric field can be calculated analytically. This is possible because for this period of time the radiated field is just the field due to a bicone whose axes are not parallel. A diagram of this problem is shown in Figure 14. A solution to the backward radiation has been provided by Latham et al<sup>14</sup>. They demonstrate that the power radiated in the backward direction in the cone  $\theta_b \leq \theta \leq \pi$  is

$$P_b = \frac{1}{2} \frac{\ln \left( \frac{\cos \beta - \cos \alpha \cos \theta_b}{\cos \alpha - \cos \beta \cos \theta_b} \right)}{\cosh^{-1} (\sin \alpha / \sin \beta)} P_i \quad (18)$$

where  $\alpha$  and  $\beta$  are the cone angles as defined in Figure 14, and  $P_i$  is the total input power. This gives the power radiated over a 1 degree cone. To get the electric field radiated we use the relationship  $P_b = E_v^2 A / \eta$ , where  $A$  is the surface area of a section of a sphere subtended by 1 degree with a radius of 1 m.

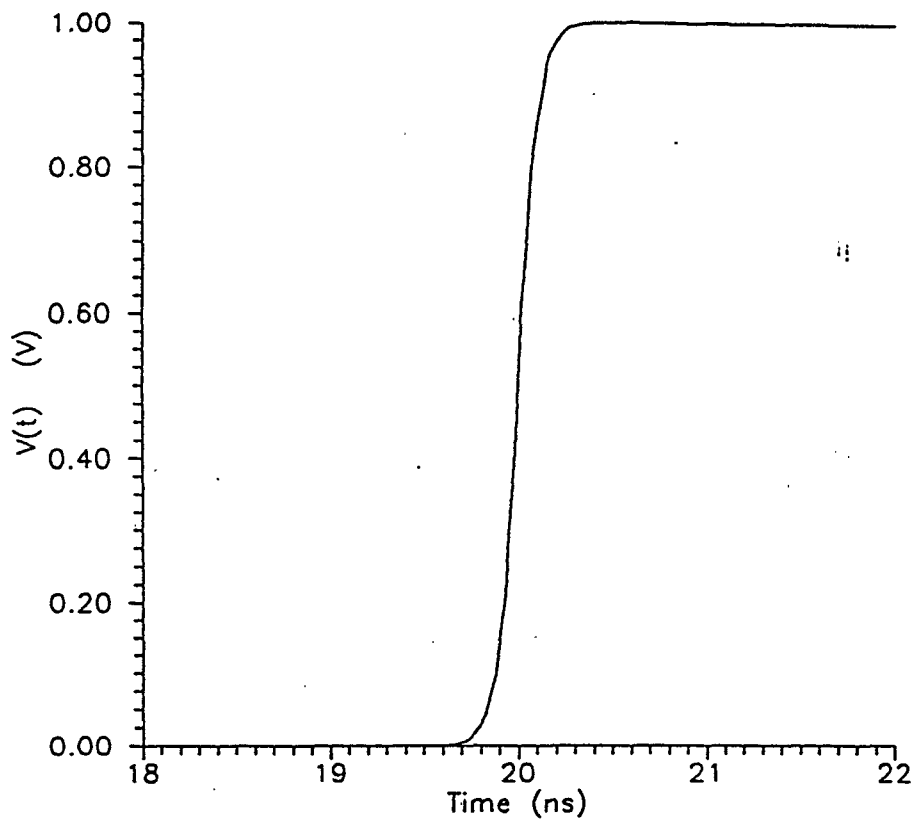
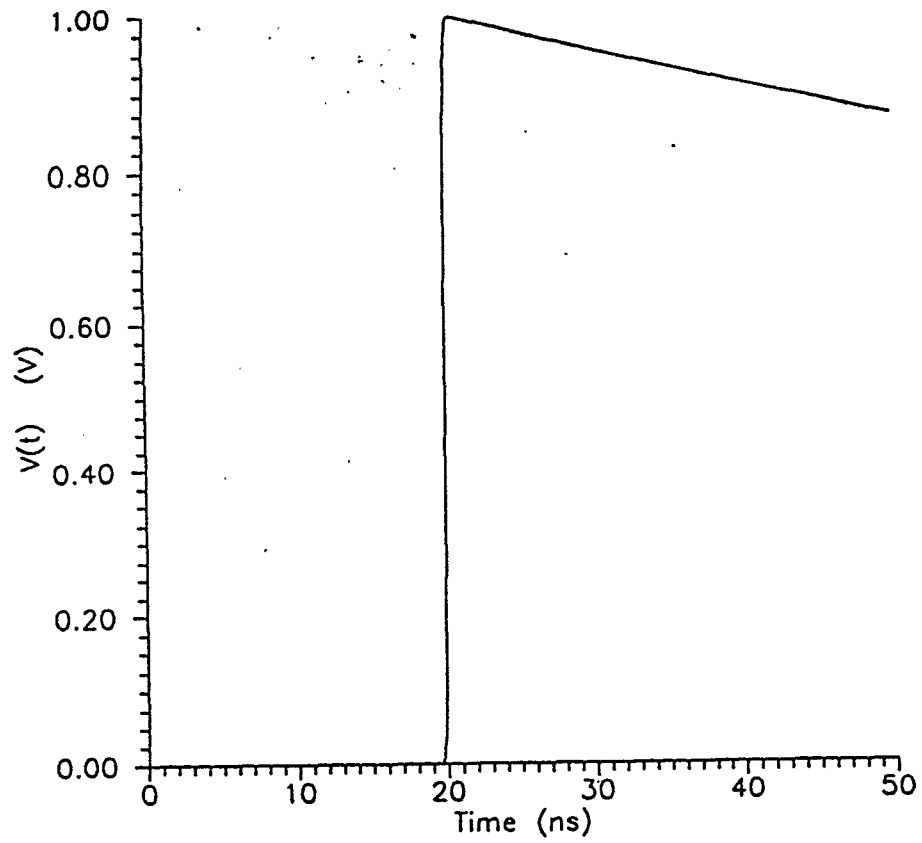


Figure 11. Inverse Double Exponential Function Used to Drive NEC

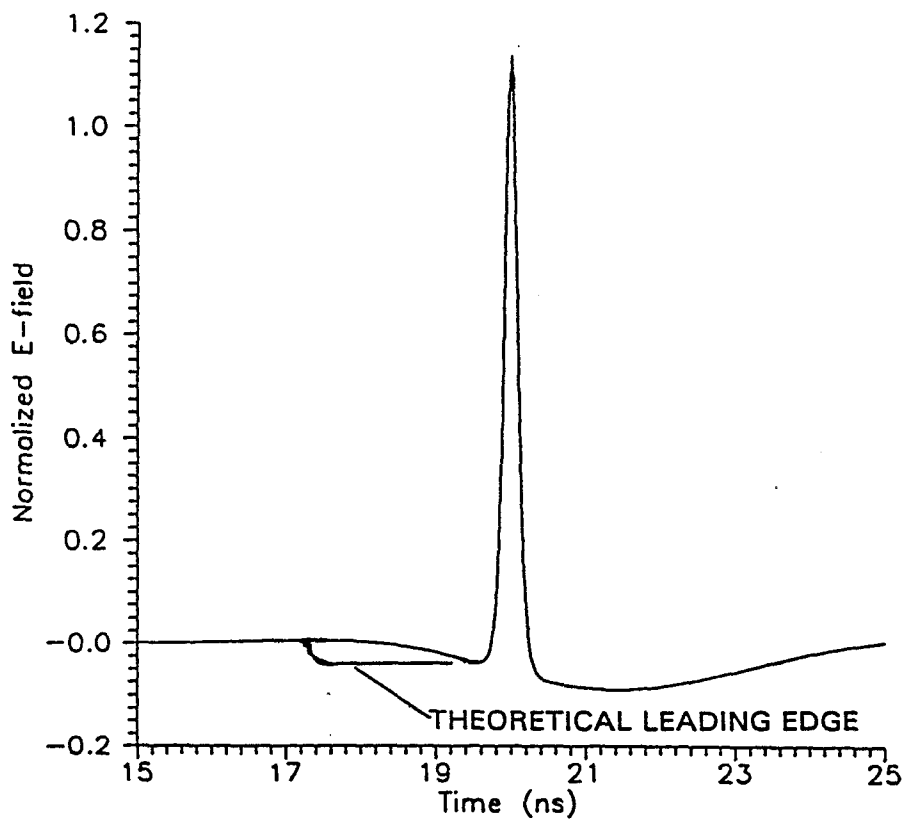
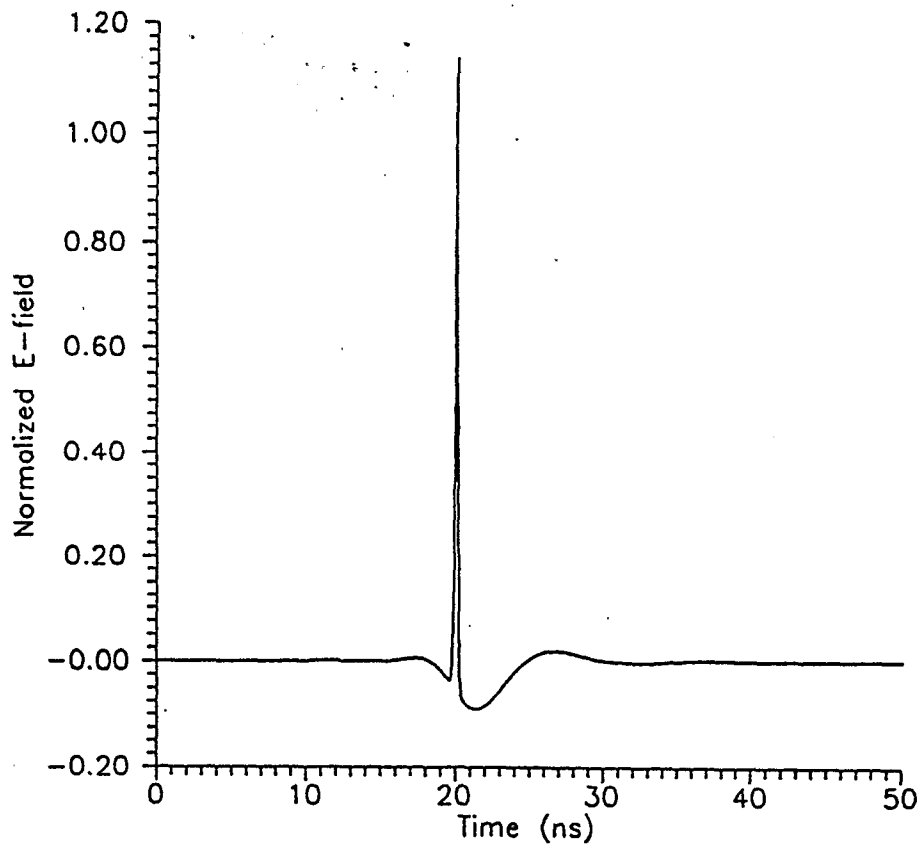


Figure 12. Radiated far-field of the IRA

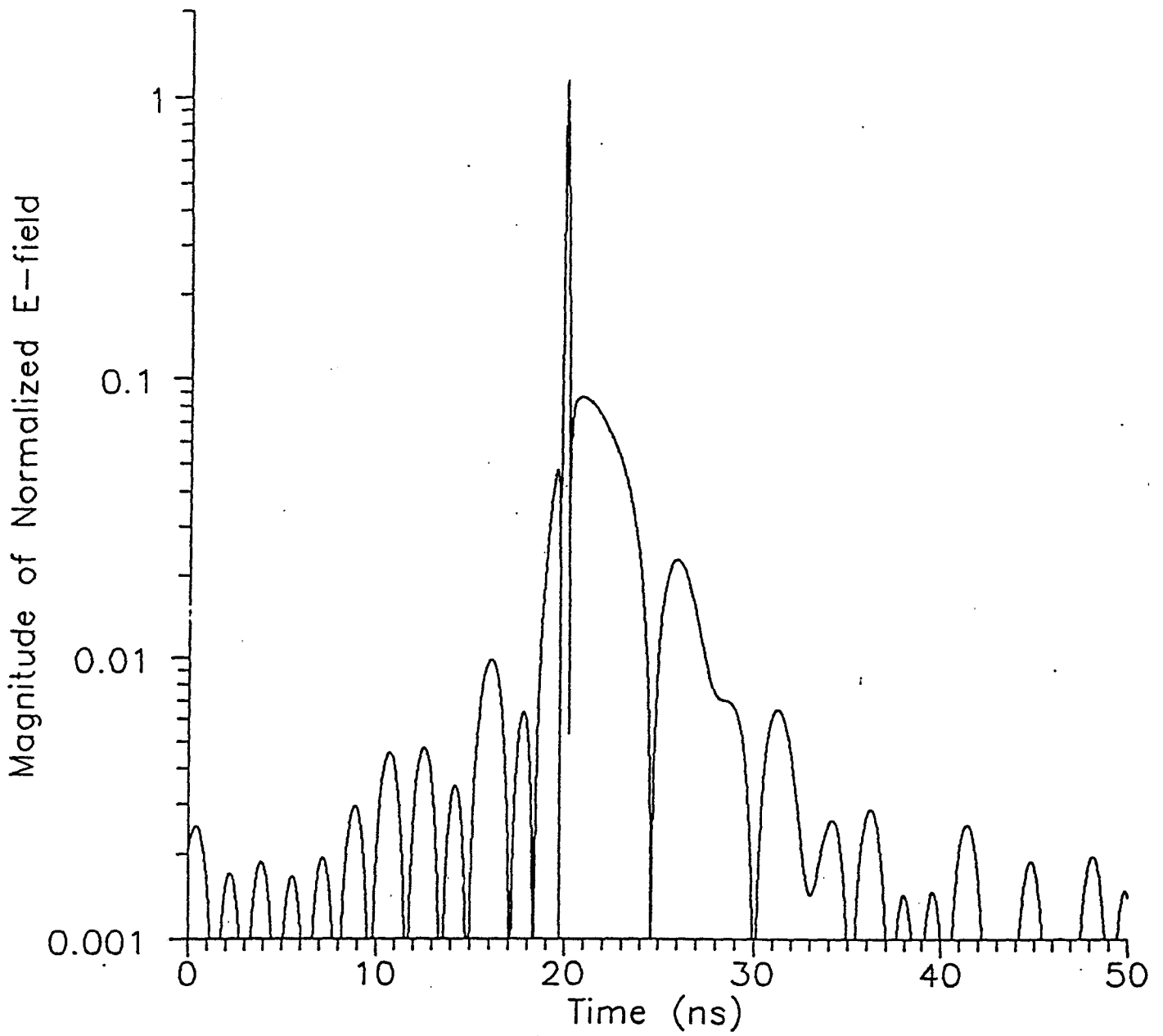


Figure 13. Radiated Far-Field of the IRA, Log Scale

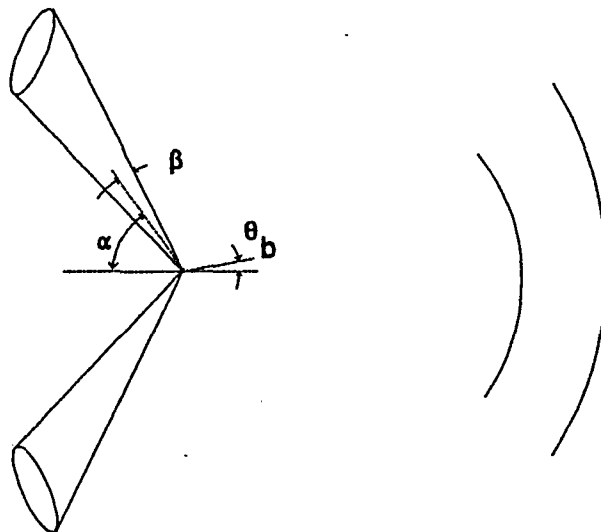


Figure 14. Geometry for the Leading Edge Calculation

If we know the field of the bent bicone in a quasistatic sense, we know the radiated far field during the clear time; i.e., the time it takes for radiation to travel from the focus to the reflector and back. From this, we can find the ratio of the peak radiated field to the leading edge. For our configuration, using the inverse double exponential with a risetime of 250 ps, we find the Peak/Leading edge ratio to be about 25. Thus, for the first 2.7 ns of the signal, the field is in the opposite direction from the peak, at a level of 1/25th of the peak. This is shown in Figure 12, where the straight line for the first 2.7 ns shows the leading edge. This can be used as an indicator of the accuracy of the NEC result. Although the NEC result attempts to show an early-time leading edge, it is not as flat or as long as we know it needs to be.

It is also of some interest to compare the output of the IRA to a hypothetical antenna that has a simple derivative waveform. If we assumed that the antenna function was just the high-frequency asymptote as calculated in Section III, we find the radiated waveform of Figure 15. Of course, this can only be hypothetical, since this waveform is always greater than zero. Real radiated waveforms have to have an integral over time equal to zero. It is nevertheless interesting how similar the hypothetical waveform is to the actual waveform.

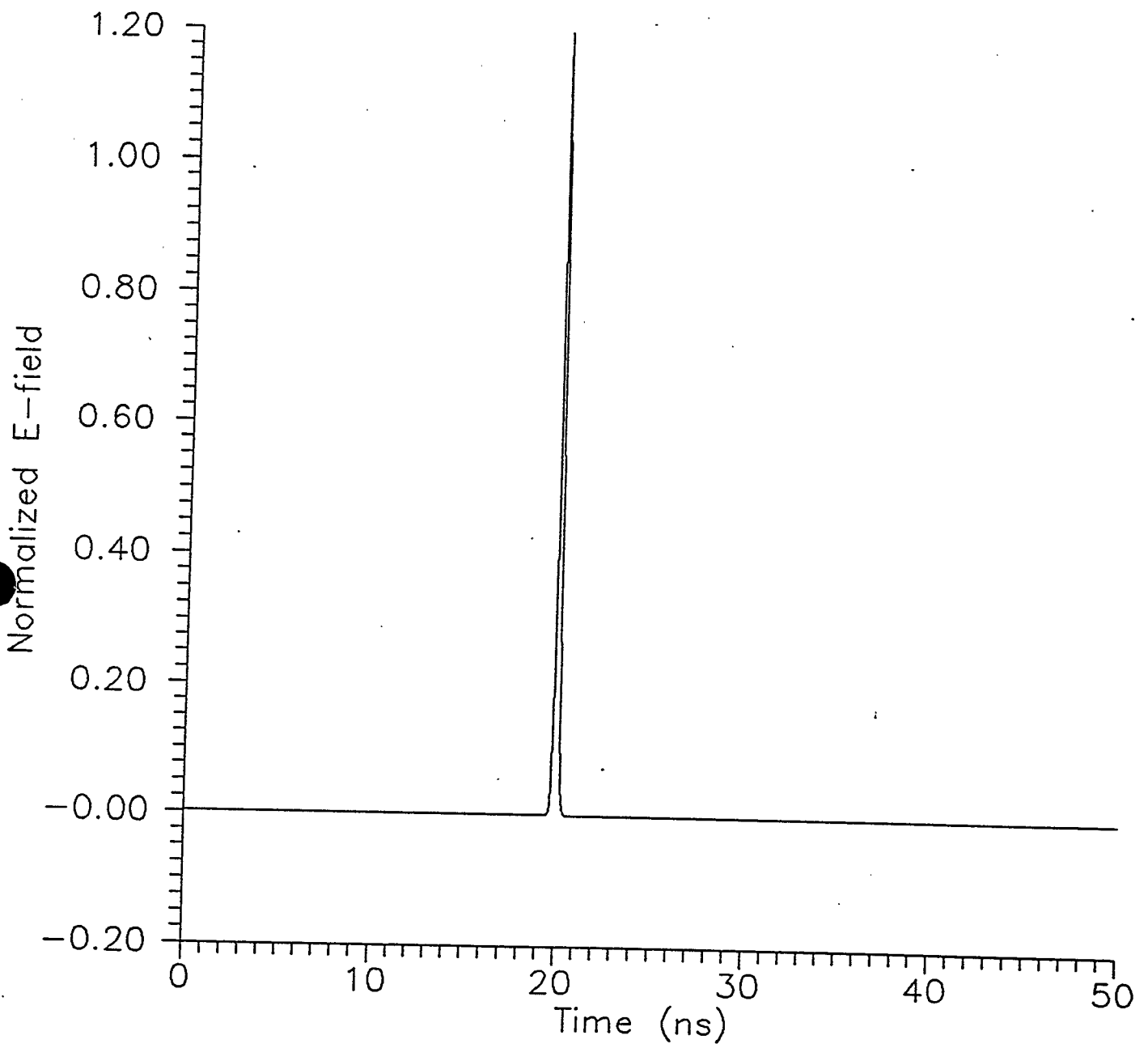


Figure 15. IRA Output Assuming a Simple Derivative Antenna Function

## VI. Conclusions and Recommendations

An antenna has been analyzed that appears to have great potential for radiating impulse-like fields. The Impulse Radiating Antenna (IRA) combines the best of high and low frequency antennas by incorporating a Balanced Transmission-line Wave (BTW) sensor to feed a dish.

An approximate analysis procedure was carried out by combining high-frequency and low-frequency techniques; i.e., the Method of Moments and Geometrical Optics. Having generated a frequency domain response of the IRA, we then drove the antenna with a step-like function and inverse transformed to get a time domain response.

Overall, the results are about what we expect. The radiated waveform closely resembles the derivative of the input voltage, however, there are extra features in the waveform associated with the need for the radiated waveform to integrate out to zero.

The next step in this investigation should consider two areas. First, there may be interest in refining the numerical models further, since experimentation is somewhat expensive. This might involve using more frequencies for the NEC calculations, and using finer detail in the modeling of the feed structure. Beside further analysis, however, the next step should include a measurement of a typical IRA. Only with a measurement will we be able to determine the nature of the approximations are in the numerical analysis. Furthermore, it seems likely that the only way to perform a complete optimization of the matching circuit will be to build the antenna and test it.

## ACKNOWLEDGEMENT

We wish to thank Dr. Carl Baum for many helpful discussions on this topic.

## References

1. M. Kanda, The effects of resistive loading of "TEM" horns, *IEEE Trans, Electromag, Compat.*, Vol EMC-24, No 2, May 1982.
2. C. E. Baum, *Radiation of Impulse-Like Transient Fields*, Sensor and Simulation Note 321, Weapons Laboratory, November 25, 1989.
3. C. E. Baum, *Configurations of TEM Feed for an IRA*, Sensor and simulation Note 327, Phillips Laboratory, April 27, 1991.
4. C.E. Baum, *Aperture Efficiencies for IRA's*, Sensor and Simulation Note 328, Phillips Laboratory, June 24, 1991.
5. E. G. Farr and J. H. Hofstra, *An Incident Field Sensor for EMP Measurements*, Sensor and Simulation Note 319, November 6, 1989, and *IEEE Trans. Electromag. Compat.*, 1991, pp. 105-112.
6. J.S. Yu, et al, *Multiple Radiations: Formation and Evaluation for Small EMP Simulators*, Sensor and Simulation Note 243, July 19, 1978.
7. C.E. Baum, *Some Characteristics of Electric and Magnetic Dipole Antennas for Radiating Transient Pulses*, Sensor and Simulation Note 125, January 25, 1971.
8. C. E. Baum, *Maximizing the Frequency Response of a B-dot Loop*, Sensor and Simulation Note 8, Air Force Weapons Laboratory, December 6, 1964.
9. W. L. Stutzman and G. A. Thiele, *Antenna Theory and Design*, Wiley, 1981, pp. 382-383.
10. C. E. Baum, *Impedances and Field Distributions for Symmetrical Two Wire and Four Wire Transmission Line Simulators*, Sensor and Simulation Note 27, Air Force Weapons Laboratory, October 10, 1966.
11. D. V. Giri and C. E. Baum, *Equivalent Displacement for a High-Voltage Rollup on the Edge of a Conducting Sheet*, Sensor and Simulation Note 294, Air Force Weapons Laboratory, October 15, 1986.
12. G.J. Burke, and A.J. Poggio, Numerical Electromagnetics Code (NEC) - Method of Moments, Lawrence Livermore National laboratory, UCID-18834, January 1981.
13. K.S.H. Lee (ed), *EMP Interaction: Principles, Techniques, and Reference Data*, 2nd Edition, Horizon, 1986, pp. 303-305.
14. R. W. Latham, et al, *Matching a Particular Pulser to a Parallel-Plate Simulator*, Circuit and Electromagnetic System Design Note 18, Air Force Weapons Laboratory, November 1974.